Check for updates

Accepted Article

# Circling in on Convective Self-Aggregation

Silas Boye Nissen*

*Niels Bohr Institute, University of Copenhagen, Blegdamsvej 17, 2100 Copenhagen, Denmark.*

Jan O. Haerter†

*Niels Bohr Institute, University of Copenhagen, Blegdamsvej 17, 2100 Copenhagen, Denmark.*

*Physics and Earth Sciences, Jacobs University Bremen, Campus Ring 1, 28759 Bremen, Germany.*

*Complexity and Climate, Leibniz Center for Tropical Marine Research, Fahrenheitstrasse 6, 28359 Bremen, Germany.*

(Dated: September 23, 2021)

In radiative-convective equilibrium simulations, convective self-aggregation (CSA) is the spontaneous organization into segregated cloudy and cloud-free regions. Evidence exists for how CSA is stabilized, but how it arises favorably on large domains is not settled. Using large-eddy simulations, we link the spatial organization emerging from the interaction of cold pools (CPs) to CSA. We systematically weaken simulated rain evaporation to reduce maximal CP radii, $R_{\max}$ and find reducing $R_{\max}$ causes CSA to occur earlier. We further identify a typical rain cell generation time and a minimum radius, $R_{\min}$, around a given rain cell, within which the formation of subsequent rain cells is suppressed. Incorporating $R_{\min}$ and $R_{\max}$, we propose a toy model that captures how CSA arises earlier on large domains: when two CPs of radii $r_{i,j} \in [R_{\min}, R_{\max}]$ collide, they form a new convective event. These findings imply that interactions between CPs may explain the initial stages of CSA.

* silas@nbi.ku.dk

† haerter@nbi.ku.dk

This article has been accepted for publication and undergone full peer review but has not been through the copyediting, typesetting, pagination and proofreading process, which may lead to differences between this version and the Version of Record. Please cite this article as doi: 10.1029/2021JD035331.

This article is protected by copyright. All rights reserved.

## I. KEY POINTS

1. Smaller cold pool radii in large-eddy simulations diminishes the time to reach convective self-aggregation.
2. We report cold pools' generation time and suppression radius by evaluating the distance between rain events connected in time.
3. A mathematical model captures the effect of domain size, suppression radius, and maximum cold pool radius in convective self-aggregation.

## II. PLAIN LANGUAGE SUMMARY

Convective self-aggregation (CSA) describes the emergence of persistently dry, cloud-free areas in numerical simulations. It has been suggested as a possible mechanism for tropical cyclone formation and large-scale events such as the Madden-Julian Oscillation. Some understanding of the persistence of CSA exists. However, how CSA initially emerges remains poorly understood. Recently, the dynamics of cold pools (CPs) have been associated with the organization of convective events. CPs are radially expanding pockets of dense air that form under precipitating thunderstorms. In this work, we ask how weakening CPs could facilitate the emergence of CSA. By analyzing high-resolution numerical simulations, we show that reducing rain evaporation shortens the time before CSA starts. These simulations demonstrate that CPs reach greater radii when rain evaporation is large. Besides, we find that new convective events occur near the point where two CPs collide. Finally, we report a minimum CP radius within which CPs are too negatively buoyant to initialize new convective events. Building on these numerical findings, we propose a simple idealized mathematical model that approximates CPs as expanding and colliding circles. We show that this model can capture the emergence of CSA. We conclude that the lack of CPs facilitates CSA.

## III. INTRODUCTION

When evaporation of rain from convective clouds is strong, so is the associated sub-cloud cooling and density increase [Simpson 1980, Engerer et al. 2008], forcing the resulting cold pools (CPs) to spread more quickly and cover larger areas [Romps and Jeevanjee 2016, Torri et al. 2015, Zuidema et al. 2017]. Such pronounced CP activity has repeatedly been suggested to hamper convective self-aggregation (CSA) in radiative-convective equilibrium (RCE) numerical experiments [Jeevanjee and Romps 2013, Muller and Bony 2015, Holloway and Woolnough 2016, Hohenegger and Stevens 2016, Yanase et al. 2020]. In these simulations, the atmosphere gradually organizes from an initially homogeneous population of convective updrafts into a segregated pattern with strongly convecting regions and dry, precipitation-free regions [Hohenegger and Stevens 2016, Held et al. 1993, Tompkins and Craig 1998, Bretherton et al. 2005, Wing et al. 2017].

Generically, CSA is characterized by the appearance of long-lived dry and warm patches within which cloud and rain are suppressed [Holloway et al. 2017]. Further drying increasingly occurs through enhanced radiative cooling in already dry regions and the resulting subsidence. Later, the dry regions expand and merge, eventually leaving only one contiguous moist area with intense low-level convergence feeding convection. Surface latent and sensible heat fluxes — which increase under stronger surface wind speed — may further increase such low-level moisture convergence.

This article is protected by copyright. All rights reserved.

Accepted Article

Physically, CPs spread as density currents along the surface, carry kinetic energy and buoyancy, and modify the thermodynamic structure near the CP edges [Tompkins 2001, Langhans and Romps 2015, de Szoeke et al. 2017]. Thereby, CPs spatially organize the convectively unstable atmosphere, establishing connections between the loci where new convective cells emerge and loci at which the previous cells dissipated. In particular, new cells were suggested to be triggered by the CP gust front alone or by collisions between gust fronts [de Szoeke et al. 2017, Glassmeier and Feingold 2017, Cafaro and Rooney 2018, Fuglestvedt and Haerter 2020]. Inspired by the notion of CP interactions, CP representations have been incorporated into large-scale models [Grandpeix and Lafore 2010], and conceptual work has formulated CPs as cellular automata [Böing 2016, Windmiller 2017, Haerter et al. 2020]. Recent work addressed the diurnal cycle of convection, where CPs effectively increased the typical length scale in the cloud field [Haerter et al. 2019]. In such an out-of-equilibrium context, mechanical lifting upon collisions of three CPs was found a dominant process, as moist boundary layer air — enclosed by gust fronts laterally — was forced to escape vertically. Triggering of new convection in such situations occurs rapidly, usually within one hour after the collision. As was shown, the three-CP collision model inevitably leads to decreased CP population over time. In RCE, slow thermodynamics processes at gust front collisions are more typical [Tompkins 2001, Fuglestvedt and Haerter 2020]. Before the onset of CSA, length scales and CP numbers are approximately conserved over time. A simple model, discussed below, capable of capturing such conserved length scales requires collisions between two rather than three CPs.

Studies on CSA often argue that sufficiently large domain sizes ($\geq 500 \times 500$ km$^2$) and coarse horizontal resolutions ($\geq 2$ km) are required for CSA [Muller and Bony 2015, Yanase et al. 2020, Bretherton et al. 2005]. To examine this claim more closely, for deliberately small domain sizes ($96 \times 96$ km$^2$) and fine horizontal resolution (200 m), we show that CSA sets in earlier when CPs are weakened through reductions in rain evaporation — that is, when the CP maximal radius, which we term $R_{\max}$, is reduced. We track the CP gust fronts to motivate that loci of gust front collisions are preferable for subsequent convective rain cells. Dependent on rain evaporation, we further detect a minimal distance $R_{\min}$ — effectively an updraft suppression radius — within which subsequent rain cells are unlikely to form, as well as a typical rain cell generation time. Using these findings, we build, simulate, and analyze a simple mathematical model, which helps understand CSA formation. We explore this model's phase diagram and find that the transition into convecting and non-convecting sub-regions occurs later for large $R_{\max}$, small $R_{\min}$, or small domain sizes $L$.

## IV. MATERIALS AND METHODS

**Large-eddy simulations.** We conducted a suite of simulations on a (96 km)$^2$ domain using the University of California, Los Angeles (UCLA) Large Eddy Simulator. The horizontal model grid is regular, and horizontally periodic boundary conditions are applied in both lateral dimensions. Vertical model resolution varies from 100 m below 1 km, stretching to 200 m near 6 km, and finally 400 m in the upper layers with 75 vertical levels in total. The Coriolis force and the mean wind were set to zero with weak, spatially uncorrelated random initial temperature perturbations, sampled uniformly within $[-0.2, 0.2]$ K for each grid box, added as noise to break complete spatial symmetry. At each output time step of 10 min, instantaneous surface precipitation intensity, specific humidity, temperature, liquid water mixing ratio, and 3D velocities are output at various model levels. We used sub-grid scale turbulence parametrized

This article is protected by copyright. All rights reserved.

Accepted Article

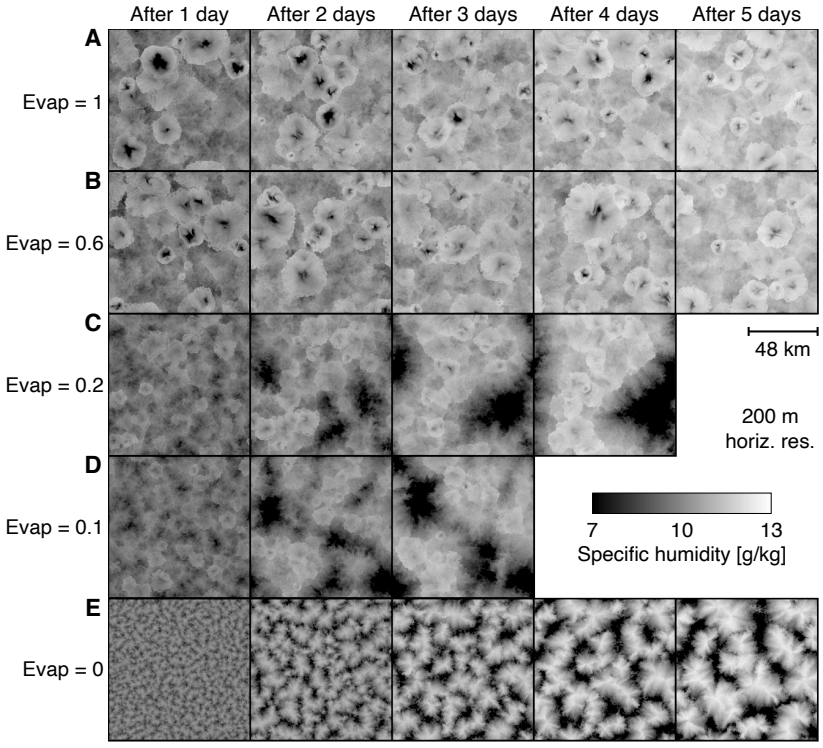


FIG. 1. **The onset of convective self-aggregation**. Near-surface specific humidity $q_v$(50 m) the first 10 min of each simulation day in radiative-convective equilibrium simulations with various degrees of rain evaporation. **(A)** Realistic rain evaporation (control simulation). **(B)** 60%, **(C)** 20%, **(D)** 10%, and **(E)** 0% rain evaporation relative to (A). Note the pronounced moisture reduction in (A–B) and the weakened moisture reduction in (C–D) within cold pool centers. Further note the evolving moisture segregation, typical of convective self-aggregation (C–D) and moisture coarsening progression (E).

after Smagorinsky [1963], delta four-stream radiation [Pincus and Stevens 2009], and a two-moment cloud microphysics scheme [Stevens et al. 2005]. Rain evaporation is accounted for by Seifert and Beheng [2006]. The five simulations have identical setups, except that the ventilation coefficient for hydrometeors is varied by fractions $\{1.0, 0.6, 0.2, 0.1, 0\}$ of its default over all vertical layers, thus influencing the rate of re-evaporation. In the following, these simulations are correspondingly labeled as "Evap=1", "Evap=0.6", etc. All simulations are run for five days, except Evap=0.2 that runs for four days, and Evap=0.1 that runs for three days (see Fig. 1). In both Evap=0.2 and Evap=0.1, the onset of CSA could already be distinguished after such shorter periods. Surface temperatures are set constant to 300 K, and insolation is fixed using a constant equatorial zenith angle of 50° to a constant 655 W m$^{-2}$ [Bretherton et al. 2005]. Surface latent and sensible heat fluxes are computed interactively and depend on the vertical temperature and humidity gradients and horizontal wind speed (bulk formula), approximated using the Monin-Obukhov similarity theory. Surface latent heat fluxes are set to 70 percent of those for a water surface. Temperature and humidity are initialized using horizontal-mean vertical profiles of temperature and humidity obtained from a prior approximately three-day spin-up using 400 m horizontal resolution (*see* Fig. S1). To explore resolution effects, we supplemented these simulations using the settings of Evap=1 repeated using horizontal resolutions of 1 km, 2 km, and 4 km, each maintaining the number of 480 × 480 horizontal grid boxes.

**Tracking of cold pools.** To track CP gust fronts, we follow the tracer particle methodology described in the

This article is protected by copyright. All rights reserved.

Accepted Article

literature [Haerter et al. 2019, Henneberg et al. 2020] using a threshold of $I_0 \equiv .5$ mm h$^{-1}$ for the rain intensity within the initial surface precipitation patch. As this tracking method is implemented to run "offline," it uses only the recorded discrete 10 min output time steps of precipitation intensity $I$ and lowest-level horizontal wind velocity ($u$(50 m), $v$(50 m)). To compare the temporal evolution of CP radii transparently between the different simulations (Fig. 2), we consider that the time of rainfall onset slightly differs between the simulations (*compare* curves in Fig. S2B). We define the time of rainfall onset as the first time point where one or more pixels have $I > I_0$. We then track all CP gust fronts present during the following 18 hours. Each CPs is followed for five hours, and the start time of all tracked CPs is aligned to produce composite statistics. The time interval of 18h was found sufficient to yield significant statistics on the spreading of each CP but short enough so that not many CP collisions were encountered. Conversely, to study collision effects (Fig. 3), we used a late-stage ($\sim$ 4 days after initialization) of the control simulation (Evap=1). For Evap=1, CP radii are large, and CPs are thus space-filling. Therefore, any new CP inevitably collides with recent CPs in its surroundings.

**Mathematical model.** The mathematical model can be described in two sentences: (1) The initial conditions: $N_1$ randomly located points on a 2D domain of size $L \times L$ with double-periodic boundary conditions expand into circles (representing cold pools) with equal and constant radial speed, $v_0$. (2) The dynamics: When two circles meet, both having their radii lie between $R_{\min}$ and $R_{\max}$ (justified in Figs. 4 and 2, respectively), the two circles instantly — at their first intersection point — initiate a new point that expands with the same radial speed, $v_0$. In other words, this model follows the principles in Haerter et al. [2019] with the major difference that two — instead of three — circles can initiate the growth of a new circle.

The outcome of this model is non-trivial. Since all circles expand with equal and constant speed, $v_0$, the dynamics allow us to categorize circles into independent *generations* that mathematically cannot interact with each other. To realize this, let us go through one example: In Fig. 5A snapshot 1, the initially $N_1$ seeded points constitute generation one, denoted as $g_1$. At slightly later snapshot 2, these points have expanded into equally sized circles that are all smaller than $R_{\min}$ and therefore do not trigger the growth of a new circle when they collide. In snapshot 3, all $g_1$ circles have grown beyond $R_{\min}$, and some have collided and initiated the start of $g_2$ circles. Since both generations continue to expand with $v_0$, circle areas corresponding to generation 2 will always lie within areas corresponding to generation 1. Therefore, in general, a $g_{i+1}$ circle cannot interact with a $g_i$ circle.

Mathematically, we define the center of the circle $i$ as $[x_i, y_i]$ and its increasing radius as $r_i$. Thereby, two circles, $i$ and $j$, are described by the following set of quadratic equations

$$(x - x_i)^2 + (y - y_i)^2 = r_i^2 \tag{1}$$

and

$$(x - x_j)^2 + (y - y_j)^2 = r_j^2 \,. \tag{2}$$

The collision point between the circles $i$ and $j$ is described by adding the distance $dr$ to both of their radii, giving

$$(x - x_i)^2 + (y - y_i)^2 = (r_i + dr)^2 \tag{3}$$

and

$$(x - x_j)^2 + (y - y_j)^2 = (r_j + dr)^2 \,. \tag{4}$$

This article is protected by copyright. All rights reserved.

Accepted Article

In the model, only collisions that fall onto the straight line between the two circle centers are allowed, assuming that this is the collision point with the highest momentum transfer, thus yielding

$$y = \frac{x - x_i}{x_j - x_i}(y_j - y_i) + y_i \,. \tag{5}$$

Eqns. 2–4 have three unknowns $(x, y, dr)$ and two solvable solutions that analytically describe the location $(x, y)$ of the collision point and when it occurs $(dr)$. One of these two solutions can be ruled out because it is either negative or non-real and, therefore, irrelevant to the model.

To implement this model computationally, we consider circles belonging to one generation at a time. For each generation, we find the pairwise distance between all circle centers. For circles whose pairwise distance is larger than $2R_{\min}$ and smaller than $2R_{\max}$, we calculate their mutual collision point by solving Eqns. 2-4 above. We sort all collision points by $dr$ and update the system by inserting circles at collision points that fulfill $R_{\min} < r_i, r_j < R_{\max}$, and are not inside a circle belonging to the current generation. When proceeding to the next generation, we return to the time point when the current generation's first circle was seeded. We note that a circle may collide with multiple circles until it reaches $R_{\max}$, and when that occurs, the circle has no further effect. We run the model until circle generation number 500, which corresponds to roughly 5000h (>200 days) given our measure of a CP generation time (∼10 hours) in Fig. 4 and similar finding in Fuglestvedt and Haerter [2020].

In Fig. 5, all simulations start with $N_1 = L^2/(10R_{\min}^2)$ points. In the supplementary material, we show that the model results are independent of the particular choice of $N_1$ (Fig. S3). Besides, we derive that given $R_{\min} = 0$ and $R_{\max} = \infty$, an initial random generation-one population $N_1$ of circles would yield $N_2 = 2N_1$ (Text S1). Subsequent growth of $N_g$ vs. $g$ would be nearly exponential, and thereby the lack of synchronous circle expansion beyond the first generation leads to a slight reduction of replication rate (Fig. S4). In other words, $R_{\min} = 0$ would result in singularities, that is, infinitely rapid non-realistic replication.

## V. RESULTS

**Weakening cold pools in RCE simulations speeds up the onset of self-aggregation.** A control simulation with realistic rain evaporation (Fig. 1A) shows no indication of CSA. We check this by computing the inter-quartile specific humidity difference (Fig. S2A), finding a weak initial increase when first CPs set in but no further increase over time. While leaving the total number of rain cells and domain-average rainfall approximately unchanged (Figs. S2B and S5A), decreasing the rate of rain evaporation (Fig. 1B–E) yields a monotonic increase in humidity variation (Fig. S2A) and overall higher near-surface temperature (Fig. S2C), along with a systematically earlier onset of persistent dry patches, e.g., near day 2 for Evap=0.2 (Fig. 1C). This comparison underlines findings from Jeevanjee and Romps [2013] and Muller and Bony [2015], who reported that CPs hamper self-aggregation. The five experiments highlight that reducing rain evaporation weakens subsidence drying in the center of CPs (*compare* dark spots in Fig. 1A–B vs. C–D) and visibly reduces CP radii. We also note that intermediate values of evaporation appear to allow for a band-like aggregation state, where rain cells form a quasi-one-dimensional chain around one of the horizontal dimensions (Fig. 1C on day 4). When rain evaporation is entirely removed (Fig. 1E), any organizing effect through CPs is absent: one is left with a coarsening process akin to reaction-diffusion dynamics [Craig and Mack 2013, Windmiller and Craig 2019], small impurities gradually merging into larger structures.

This article is protected by copyright. All rights reserved.

Accepted Article

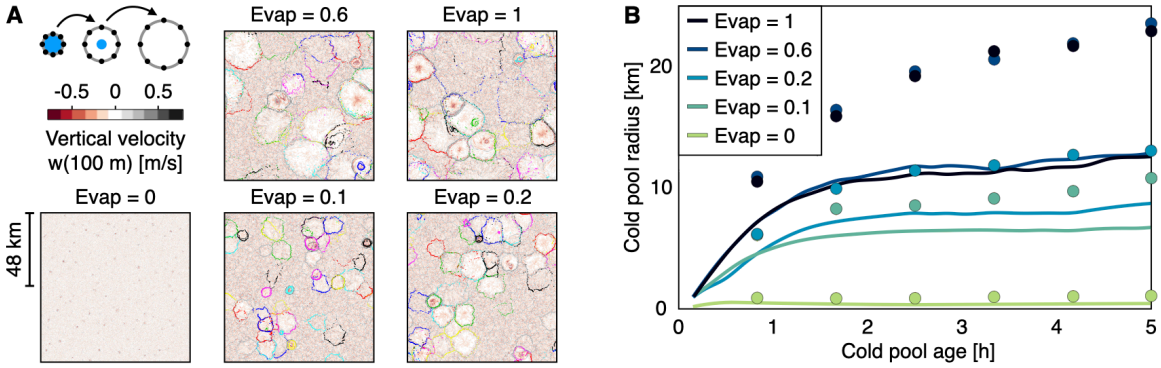


FIG. 2. **Maximum radius, $R_{max}$. (A)** Tracking all cold pool (CP) gust fronts present during the first 18h of precipitation. Top-left cartoon: we track a CP gust front (grey rim) by placing tracers (black points) around the rain event (blue spot) and let the tracers move radially away from the rain event with the horizontal wind (*Details:* Methods). Each panel shows the near-surface vertical velocity field 18h after precipitation onset and gust front tracers marked by colors indicating different CPs. **(B)** Composite (average) CP radii as the CPs evolve after their emergence (lines) and the 90th radius percentile (dots). Note that CPs initially grow quickly but monotonically slow and that the maximal CP radii increase with rain evaporation rate.

**Measuring the maximum cold pool radius, $R_{max}$.** Using a rain cell [Moseley et al. 2019] and CP [Haerter et al. 2019, Henneberg et al. 2020] tracking method, we seed tracer particles at the boundary of surface rain patches (Fig. 2A, top-left cartoon). We advect these tracers using the radial velocity field, forcing them to gather in pronounced convergence areas caused by the CP gust fronts (*Details:* Methods). Superimposing the resulting pattern of tracers onto the near-surface vertical velocity field (Fig. 2A) confirms that the tracers gather along the edge of each CP (subsident or featureless vertical wind field). By plotting the average time evolution of the CP radii in each simulation (Fig. 2B), we find that for Evap=1, CPs on average expand to 11 km five hours after initiation with the 90th radius percentile reaching 23 km. This value is comparable to previous simulation results found on various domain sizes [Romps and Jeevanjee 2016, Tompkins 2001] and observational findings [Black 1978, Zuidema et al. 2012, Feng et al. 2015]. Reducing evaporation results in systematically smaller CP radii: for Evap=0.2, CPs on average reach 8 km in radii during the same time with 90th percentile reaching 13 km, and for Evap=0, CP radii equal the corresponding surface rain cells, as, without CPs, there is no pronounced wind field to advect the tracers.

**New convective events are initiated in the vicinity of cold pool collisions.** What is then the specific role of CPs in maintaining domain-wide convection? To explore this, first consider locations of rainfall at a particular time step of Evap=1 (Fig. 3A), the associated cloud-base vertical velocity (Fig. 3B), and specific humidity (Fig. 3C). Updrafts form shortly before the onset of rainfall. In contrast, specific humidity becomes elevated earlier — in line with RCE simulations, where a considerable moisture build-up before any subsequent convective event was reported [Fuglestvedt and Haerter 2020]. Second, we determine gust front loci using CP tracer particles, which have been shown to gather at the intersections between CPs [Haerter et al. 2019, Henneberg et al. 2020]. The humidity during rain event build-up (peak highlighted in Fig. 3C) is elevated by approximately 0.3 to 0.4 g/kg compared to the domain mean (bold horizontal line in the panel). Using the tracers to collect, as a comparison, the specific humidity at CP gust fronts, it is found that this histogram is similarly shifted to moister values (Fig. 3D, *compare* green vs. black curve). In summary, loci of CP collisions do provide the positive humidity anomalies typical of subsequent convective events.

This article is protected by copyright. All rights reserved.

Accepted Article

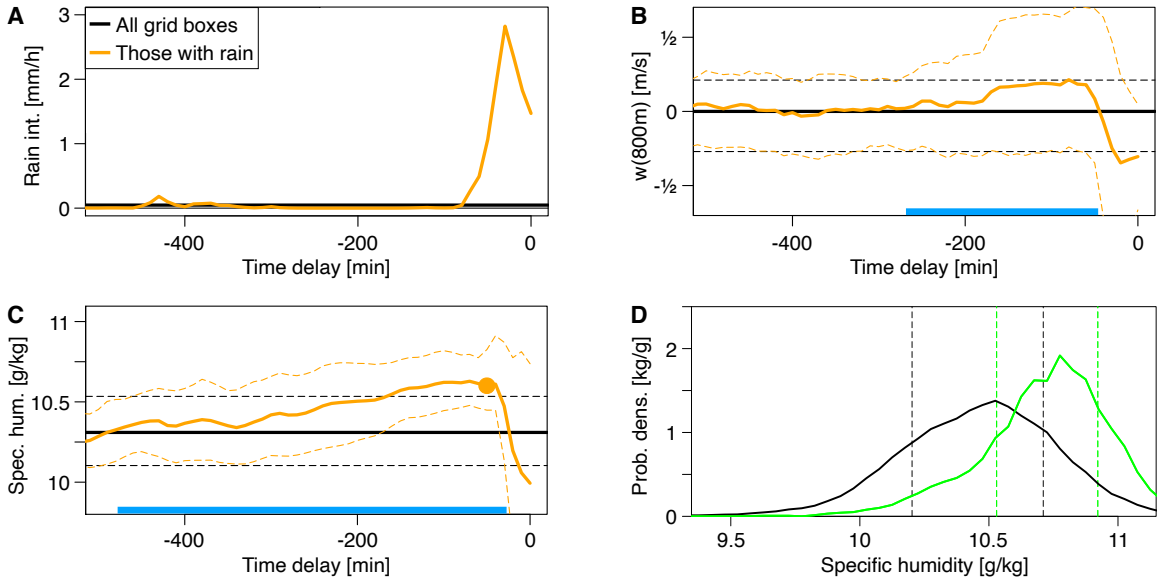


FIG. 3. **Identifying cold pool collisions**. The time $t = 0$ is defined as 1670 minutes after model initialization, a time point sufficiently close to the onset of precipitation in Evap=1 ($\approx$ 600 min) but sufficiently long after the onset so that the histories of rain intensity, vertical velocity, and specific humidity can be tracked. **(A)** History of rain intensity conditionally averaged over all grid boxes with rainfall at $t = 0$ (orange) and domain mean rainfall (black) for the simulation Evap=1. **(B)** Analogous to A, but for vertical velocity near the cloud base ($w$(800 m)). The domain average is zero throughout. Thin lines mark corresponding 20th and 80th percentiles. The blue bar highlights the time during which updrafts exceed the domain average. Note the pronounced peak, corresponding to convective updrafts, as is expected before rain onset, and the dip near $t = 0$, corresponding to CP-associated downdrafts. **(C)** Analogous, but for near-surface specific humidity, $q_v(z = 50$ m). The blue bar highlights the time during which specific humidity exceeds the domain average. Note the relatively long build-up of humidity before rainfall onset. **(D)** Histograms of $q_v$(50 m) at $t = 0$ for all data (black curve) and gust front positions only (green curve).

**New deep convective events are initiated at a certain distance, $\mathbf{R_{min}}$, away from earlier events.** To quantify a possible suppression effect caused by a present rain cell's CP on subsequent cells forming within the surroundings, we examine whether rain events are spaced uniformly after the initial rain onset. A non-uniform spacing would imply either suppression (larger distance) or activation (smaller distance), whereas a uniform spacing would speak against a direct spatial influence on subsequent rain cell formation. We thus identify all rain events within the first 12h after rain onset [Moseley et al. 2013], allowing us to compare non-aggregating simulations with aggregating simulations (day 1 in Fig. 1). We measure each rain cell's distance to its nearest rain event occurring within a time window $\Delta t$.

As a control, we use that the probability for $n$ points to all lie outside a circle of radius $d$ is $(1-\pi d^2/L^2)^n$, where $L$ is the domain length and $n$ is the number of rain events during $\Delta t$. Differentiating this with respect to $-d$ gives the probability density function $f(d) = 2n\pi d(1-\pi d^2/L^2)^{n-1}/L^2$, from which we compute the expected nearest-neighbor distance given a uniform distribution of points (orange curves in Fig. 4). Comparing this to the simulation data (blue curves in Fig. 4), we find an inhibitory effect causing the nearest neighbor distance to be larger than 5 km for up to 8h. We refer to this distance as $R_{\min} \approx 6$ km and explain it by CPs being too negatively buoyant to initialize new

This article is protected by copyright. All rights reserved.

Accepted Article

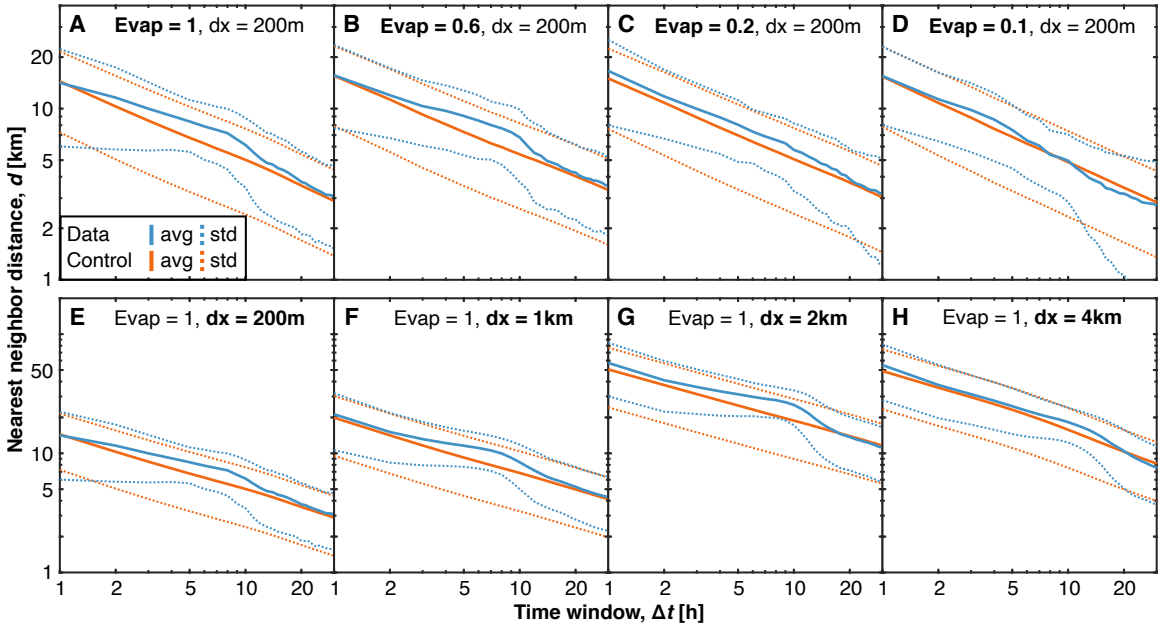


FIG. 4. **Generation time and an effective minimal radius, $R_{min}$. (A–D)** The average distance ($d$) between rain events occurring within the first 12h past precipitation onset and their nearest neighbor rain event (blue) occurring within a time window ($\Delta t$) for varying evaporation rates (Evap). We contrast that to a control where the same number of rain events are located uniformly (red). The dotted lines mark the standard deviations. More rain events are included for larger time windows, causing the distances to be smaller. In (A), note the lack of events within 6 km for up to 8h. **(E–H)** Analog, but for varying horizontal resolutions ($dx$). Note the inhibitory distance increases for coarser horizontal resolutions without changing the time scale at which it occurs.

convective cells within this distance [Drager and van den Heever 2017, Fournier and Haerter 2019]. We find that this spatial scale is independent of the rain evaporation rate (Fig. 4A–D), but it increases for coarser horizontal resolutions (Fig. 4E–H). A possible explanation for the latter lies in decreasing rain event number densities (Fig. S5B). A caveat in quantifying rain event number densities lies in using a proper definition of rain events at different model resolutions. A common intensity threshold, as we have pragmatically used here, can be debated. Tompkins and Semie [2017] performed a similar nearest neighbor analysis on RCE simulations with a 2 km horizontal resolution. They found that CPs suppress rain events within 20 km of range, supporting our results in Fig. 4G. Besides denoting the suppression at small timescales ($\Delta t \lesssim 10$h) to CPs, they further assigned the activation at larger timescales ($\Delta t \gtrsim 10$h) to CSA – an effect we see most clearly in Fig. 4D, which aggregates within three days (Fig. 1D).

When increasing the time window of included events beyond $\Delta t = 10$h, we find that this suppression effect diminishes; that is, the distribution function approaches a uniform distribution (Figs. 4 and S6). On this time scale, the CPs associated with two rain events have time to grow larger than $R_{\mathrm{min}}$, collide, and trigger the formation of a new, closer rain event belonging to the subsequent generation. We, therefore, interpret the time scale ∼10 hours as the generation time of one CP. Our data indicate that this time scale slightly decreases for decreasing evaporation rates, likely because those simulations are transitioning to CSA (Fig. S6A–D). Many rain events must be initiated within a relatively small area in the self-aggregated state, thus locally driving up the frequency at which new cells are generated. Finally, we find that the same time scale slightly increases for coarser horizontal resolution, likely due to

This article is protected by copyright. All rights reserved.

Accepted Article

higher average rain intensities per rain event triggering stronger CPs that last for a longer time (Fig. S6E–H).

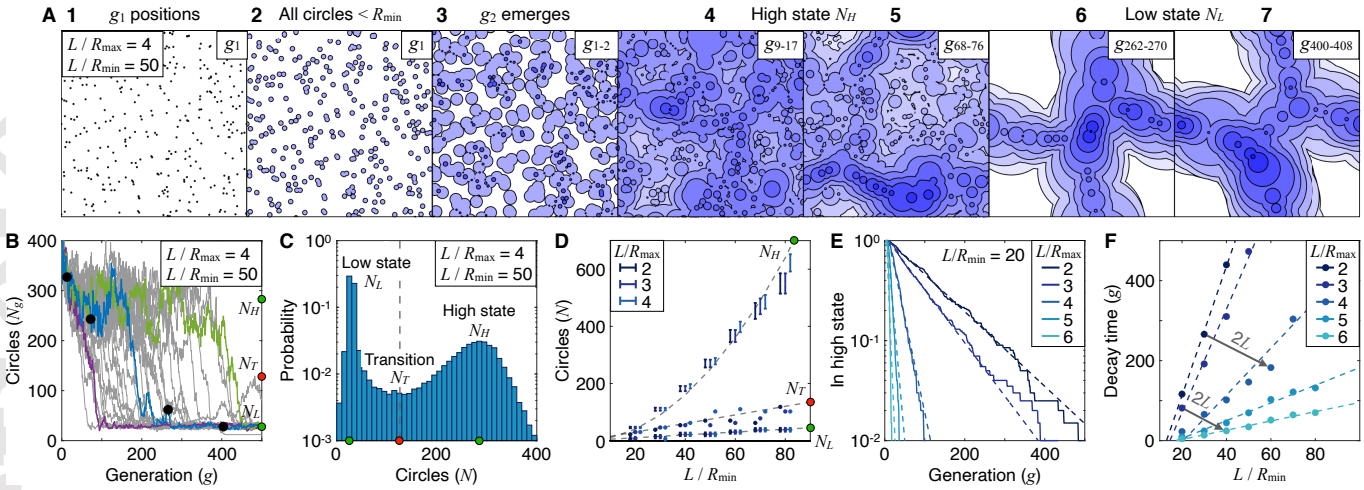


FIG. 5. **Circle model. (A)** Seven snapshots running forward in time from one model run with $L/R_{\max} = 4$ and $L/R_{\min} = 50$. Snapshots 1–2 show the initial $g_1$ positions. Snapshot 3 shows the emergence of $g_2$ circles (cold pools). Snapshots 4–5 and 6–7 show representative pictures of the high state ($N_H$) and the low state ($N_L$), respectively (*Details:* Methods). Within each snapshot, circles of the same color belong to the same generation ($g$), and white (dark blue) areas correspond to the most historic (recent) generations. **(B)** The number of circles ($N_g$) per generation ($g$) as 30 simulations with varying initial $g_1$ positions evolve. Three runs are highlighted. The blue curve represents the simulation in (A), and the black dots indicate the time points of the last four snapshots in (A). Note the existence of two qualitatively distinct states of high and low $N_g$ marked with green dots as $N_H$ and $N_L$, respectively. The red dot, $N_T$, marks the transition point. **(C)** The distribution of circles in all generations pooled together for 200 runs. In (A–C), $L/R_{\max} = 4$ and $L/R_{\min} = 50$. **(D)** The number of circles in the low $N_L$ and high $N_H$ states and at the transition point $N_T$ for varying $L/R_{\max}$ and $L/R_{\min}$. **(E)** The fraction of runs in the high state as generation number for $L/R_{\min} = 20$. Note the logarithmic vertical axes. **(F)** The characteristic decay time as a function of $L/R_{\max}$ and $L/R_{\min}$. Note that higher $L$, higher $R_{\min}$, or lower $R_{\max}$ result in faster decay.

**A simple mathematical model captures the onset of self-aggregation.** To understand the role of CP collisions, we introduce a model consisting of growing and colliding circles that represent the gust fronts of CPs (*Details:* Methods). The reasoning is that in RCE, most new rain cells result from thermodynamic pre-conditioning near the gust front collision lines (Fig. 3; see also Fuglestvedt and Haerter [2020]. Besides, the delay between the collision time and the initiation of the resultant rain cell is so large (typically several hours) that direct forced lifting can be ruled out. In line with the findings in Fig. 4, CPs with $r < R_{\min}$ are considered too negatively buoyant to initialize new CPs [Drager and van den Heever 2017, Fournier and Haerter 2019], and CPs with $r > R_{\max}$ are considered too weak to trigger new events.

The dynamics during the first two generations are introduced in the *Methods* section (Sec. IV). After approximately ten generations, new circles are initiated throughout the domain with no obvious patterning (Fig. 5A snapshots 4–5) — we term this the "high state" having $N_H$ circles. Later, a separation into a circle-filled (convecting) and a circle-free (non-convecting) sub-region occurs (Fig. 5A snapshots 6–7) — we term this the "low state" having $N_L$ circles. Note the visual similarity with the numerical experiment in Fig. 1C–D. The number of circles $N_g$ in all simulations eventually drops from high to low (Fig. 5B). The histogram of $N$, which is bimodal, confirms the notion of two distinct meta-stable states (Fig. 5C). By "meta-stable state," we thereby refer to a state resistant to small perturbations but

This article is protected by copyright. All rights reserved.

Accepted Article

non-resistant to larger perturbations.

We now explore how the two states depend on the independent model parameters $L/R_{\min}$ and $L/R_{\max}$. We find that the number of circles in the low state, $N_L$, scales as $N_L = L/(2R_{\min})$, whereas that in the high state, $N_H$, scales as $N_H = L^2/(10R_{\min}^2)$, both independent of $R_{\max}$ (Fig. 5D). The transition point occurs at $N_T \approx 1.5L/R_{\min}$. The linear scaling $N_L \sim L$ is commensurate with band-like, one-dimensional structures (compare Fig. 5A snapshots 6–7 and Fig. 1C–D on days 2–4). In contrast, $N_H \sim L^2$ is in line with two-dimensional organization. By fitting the fraction of simulations in the high state to an exponential function (Fig. 5E), we show that a characteristic time exists when the simulations decay to the low state. Thereby, we find that the circle model predicts decreasing $R_{\max}$, increasing $L$, or increasing $R_{\min}$ speed up the characteristic time when the transition occurs (Fig. 5F). Decreasing $R_{\max}$ is in correspondence with the results presented in Figs. 1–2, increasing $L$ has previously been reported to facilitate self-aggregation [Muller and Bony 2015, Bretherton et al. 2005], and rising $R_{\min}$ is due to coarser horizontal resolution (Fig. 4E–H) favoring self-aggregation [Yanase et al. 2020, Hirt et al. 2020].

## VI. DISCUSSION AND CONCLUSION

There is convincing evidence for the crucial role played by radiative feedbacks in increasing and maintaining a horizontal dry-moist imbalance in a RCE atmosphere [Muller and Bony 2015, Bretherton et al. 2005, Wing et al. 2017, Tompkins 2001, Muller and Held 2012, Emanuel et al. 2014]. In particular, Emanuel et al. [2014] presented a simplified theoretical model for water vapor-radiation-circulation feedbacks, in which a linear instability exists that can reinforce initial moisture imbalance once formed. Muller and Bony [2015] support this view and highlights the role of clouds and cold pools. Theories have also been proposed for Turing-instability type coarsening of the RCE atmosphere into moist and dry sub-regions driven by feedbacks in radiation and surface fluxes [Craig and Mack 2013]. Yet, these classical studies on CSA either use relatively coarse horizontal grid spacing, such as 3 km in Bretherton et al. [2005], or assume the boundary layer moisture to be horizontally homogeneous [Emanuel et al. 2014]. These model features lead to weakened or absent representation of CP effects, which are crucial in impacting CSA [Jeevanjee and Romps 2013]. The notion that CP collisions trigger new convective events is well documented [Purdom 1976, Weaver and Nelson 1982, Torri and Kuang 2019] and addressed in toy models [Böing 2016, Haerter 2019].

To capture the potential role of CPs during the onset of CSA, we here explicitly model the two-particle interaction resulting from interacting CP gust fronts. To incorporate the buoyancy suppression effect within the center of each CP, we introduce the radius $R_{\min}$, within which no activation is possible. Such a suppression radius would act against any local positive moisture feedbacks that would favor new rain cells to form close to previous ones. Our study investigates how $R_{\min}$ and the maximal CP radius $R_{\max}$ could influence the ability of an initially scattered rain cell and CP population to eventually facilitate dry regions — which could then grow to give rise to CSA. The circle model implies that large CPs, as formed by pronounced rain evaporation, become space-filling where CPs fill the whole domain, and there is a connected, percolating patch through the domain among CPs from the same generation. From hexagonal close-packing, that is, circles organized on a triangular lattice, where each circle exactly touches its six neighboring circles, $L/(2R_{\max})$ circles can be placed along one dimension, and $L/(\sqrt{3}R_{\max})$ circles can be placed along the other dimension. This gives a lower radius bound for space-filling $R_{\max} > L(2\sqrt{3}N)^{-1/2} \approx 7.3$ km, where $L = 96$ km is the domain length, and $N \approx 50$ is the number of CPs per generation (Fig. S5A). For radii smaller than

This article is protected by copyright. All rights reserved.

Accepted Article

this, areas emerge that newly initialized circles cannot reach — a gap results, and the transition to CSA starts. When (realistically) departing from perfect close-packing, the required value of $R_{\max}$ is larger — commensurate with our findings (Fig. 2) and the transition to CSA between Evap=0.6, where $R_{\max} \approx 11$ km, and Evap=0.2, where $R_{\max} \approx 8$ km.

Similar percolation-based arguments could be made for cloud-resolving numerical experiments carried out at coarser horizontal resolution, where CSA was found to be favored compared to fine resolution. At coarse resolution, the number of rain cells may be reduced at the benefit of the rain volume achieved by each rain cell. Percolation may thus be harder to achieve, and dry patches would be more likely to result (Fig. S5B). However, we point out that a follow-up on this point requires careful consideration of how to set a meaningful rain intensity threshold when defining and comparing rain events with differing model resolutions.

Our model simplifies CP expansion by assuming constant radial expansion speed, $v_0$. In reality, CPs initially grow quickly, and their expansion speed decreases gradually over a few hours (Fig. 2B) [Grant and van den Heever 2016, 2018]. Introducing a smoothly varying gust front speed into our model would require a time-dependent expansion speed factor, and a numerically approximate approach is more practicable [Haerter et al. 2019]. The presented model does not reach a final, fully-aggregated state, where a small fraction of the domain intensely convects indefinitely. This sustained activity might be obtained by adding spatial noise (displacing new circles slightly away from the exact geometric collision point) and systematically increased triggering probabilities for decreased overall rain area [Haerter 2019]. Extensions could include explicit incorporation of the "super-CP" [Windmiller and Hohenegger 2019] and radiatively driven CP [Yanase et al. 2020, Coppin and Bony 2015], constituting the two components of the final large-scale circulation. This model extension would allow triggering events at the edges of the intensely convecting sub-region due to convective CPs colliding with the opposing radiatively driven CP — a mostly dynamics effect. Such circulation feedbacks may well be essential in stabilizing the final steady-state but may not be required to develop the first dry patches and their initial growth, which we have focused on in this work.

Nearly conserved rain cell numbers (Fig. S5A) and rain intensities (Fig. S2B) are supported by radiation constraints on precipitation in RCE [Held and Soden 2006]. This conservation can be reached by accounting for an additional feedback mechanism: triggering new rain cells by existing CPs may be more dynamic, as the convective instability within the moist convective sub-region will likely be increased at the expense of the subsiding dry sub-region. The time delay between CP collisions and dynamical triggering of new convective cells takes $\mathcal{O}(1h)$ [Haerter et al. 2019], which is an order of magnitude less than the entire generation time of CPs during the early non-aggregated state, $\mathcal{O}(10h)$ (Fig. 4 and Fuglestvedt and Haerter [2020]). Our model could be further developed to explicitly incorporate a time delay between any CP collision and the initiation of the subsequent CP expansion at the location of the collision. For example, this time delay could be chosen proportional to the number of CPs present at a given time.

In conclusion, our simple model captures various characteristics of the onset of convective self-aggregation (CSA): reduced rain evaporation and larger domain sizes speed up the start of CSA in cloud-resolving simulations, consistent with reduced $R_{\max}$ and increased $L$ in our circle model. Finally, our model makes the testable prediction that increased suppression radius $R_{\min}$ promotes an early onset of CSA. A corresponding exploration of the parameter space in large-eddy and cloud-resolving simulations would be computationally costly, as not only a range of system sizes and rain re-evaporation rates would need to be explored. Additionally, each parameter combination would require an initial condition ensemble due to the potentially stochastic transition between the high and low CP density states. Our

This article is protected by copyright. All rights reserved.

Accepted Article

results could guide an exploration of the parameters mentioned. In particular, the exponentially decaying residence likelihood in the high state (Fig. 5E) implies a stochastic process, where a transition is possible at equal probability $r$ within each generation, that is, $\dot{N}_H \sim -rN_H$. Such a stochastic process could be probed within a reduced set of large-eddy or cloud-resolving simulations. If verified, it should be explored, if such a stochastic process also carries over to spatially-independent CP processes, at a scale properly chosen to be significantly larger than the typical CP diameter — that is, if cavities can emerge at any sub-region of the model domain statistically-independently of other sub-regions. Physically, one could alternatively perform a scale analysis of the larger-scale circulation at different vertical levels to characterize the long-wavelength modes that are present immediately before the onset of CSA. If such long-wavelength modes are well below system size, one may be able to conclude that local processes, such as CP effects, indeed constitute the cause of initial dry patch formation.

## ACKNOWLEDGMENTS

We thank Steven J. Böing, Cathy Hohenegger, Ronja Gronemeyer, and the Atmospheric Complexity Group at the Niels Bohr Institute for discussions. We thank Adrian Tompkins and one additional anonymous reviewer for valuable comments on our manuscript. The large-eddy simulation data and the source code for the circle model (implemented in MATLAB) are available at `http://doi.org/10.5281/zenodo.5228449`. SBN acknowledges funding through the Danish National Research Foundation (grant number: DNRF116). JOH gratefully acknowledges funding by a grant from the VILLUM Foundation (grant number: 13168) and the European Research Council (ERC) under the European Union's Horizon 2020 research and innovation program (grant number: 771859). We acknowledge the Danish Climate Computing Center (DC3) and thank Roman Nuterman for his technical support. The authors gratefully acknowledge the German Climate Computing Centre (Deutsches Klimarechenzentrum, DKRZ).

## AUTHOR CONTRIBUTIONS

JOH ran and processed the large-eddy simulations, tracked the rain cells and cold pools, and contributed to the manuscript. SBN analyzed the simulation data, developed, implemented, analyzed the circle model, and drafted and revised the manuscript.

## COMPETING INTERESTS

The authors declare no competing interests.

---

Joanne Simpson. Downdrafts as linkages in dynamic cumulus seeding effects. *Journal of Applied Meteorology*, 19(4):477–487, 1980.

Nicholas A Engerer, David J Stensrud, and Michael C Coniglio. Surface characteristics of observed cold pools. *Monthly Weather Review*, 136(12):4839–4849, 2008. doi:https://doi.org/10.1175/2008MWR2528.1.

This article is protected by copyright. All rights reserved.

Accepted Article

David M Romps and Nadir Jeevanjee. On the sizes and lifetimes of cold pools. *Quarterly Journal of the Royal Meteorological Society*, 142(696):1517–1527, 2016. doi:https://doi.org/10.1002/qj.2754.

Giuseppe Torri, Zhiming Kuang, and Yang Tian. Mechanisms for convection triggering by cold pools. *Geophysical Research Letters*, 42(6):1943–1950, 2015. doi:https://doi.org/10.1002/2015GL063227.

Paquita Zuidema, Giuseppe Torri, Caroline Muller, and Arunchandra Chandra. A survey of precipitation-induced atmospheric cold pools over oceans and their interactions with the larger-scale environment. *Surveys in Geophysics*, pages 1–23, 2017. doi:https://doi.org/10.1007/s10712-017-9447-x.

Nadir Jeevanjee and David M Romps. Convective self-aggregation, cold pools, and domain size. *Geophysical Research Letters*, 40(5):994–998, 2013. doi:https://doi.org/10.1002/grl.50204.

Caroline Muller and Sandrine Bony. What favors convective aggregation and why? *Geophysical Research Letters*, 42(13): 5626–5634, 2015. doi:https://doi.org/10.1002/2015GL064260.

Chris E Holloway and Steven J Woolnough. The sensitivity of convective aggregation to diabatic processes in idealized radiative-convective equilibrium simulations. *Journal of Advances in Modeling Earth Systems*, 8(1):166–195, 2016. doi: https://doi.org/10.1002/2015MS000511.

Cathy Hohenegger and Bjorn Stevens. Coupled radiative convective equilibrium simulations with explicit and parameterized convection. *Journal of Advances in Modeling Earth Systems*, 8(3):1468–1482, 2016. doi:https://doi.org/10.1002/2016MS000666.

Tomoro Yanase, Seiya Nishizawa, Hiroaki Miura, Tetsuya Takemi, and Hirofumi Tomita. New critical length for the onset of self-aggregation of moist convection. *Geophysical Research Letters*, 47(16):e2020GL088763, 2020. doi: https://doi.org/10.1029/2020GL088763.

Isaac M Held, Richard S Hemler, and V Ramaswamy. Radiative-convective equilibrium with explicit two-dimensional moist convection. *Journal of the Atmospheric Sciences*, 50(23):3909–3927, 1993.

Adrian M Tompkins and George C Craig. Radiative–convective equilibrium in a three-dimensional cloud-ensemble model. *Quarterly Journal of the Royal Meteorological Society*, 124(550):2073–2097, 1998. doi:https://doi.org/10.1002/qj.49712455013.

Christopher S Bretherton, Peter N Blossey, and Marat Khairoutdinov. An energy-balance analysis of deep convective self-aggregation above uniform SST. *Journal of the Atmospheric Sciences*, 62(12):4273–4292, 2005. doi: https://doi.org/10.1175/JAS3614.1.

Allison A Wing, Kerry Emanuel, Christopher E Holloway, and Caroline Muller. Convective self-aggregation in numerical simulations: a review. *Surveys in Geophysics*, 38(6):1173–1197, 2017. doi:https://doi.org/10.1007/s10712-017-9408-4.

Christopher E Holloway, Allison A Wing, Sandrine Bony, Caroline Muller, Hirohiko Masunaga, Tristan S LEcuyer, David D Turner, and Paquita Zuidema. Observing convective aggregation. *Surveys in Geophysics*, 38(6):1199–1236, 2017. doi: https://doi.org/10.1007/s10712-017-9419-1.

Adrian M Tompkins. Organization of Tropical Convection in Low Vertical Wind Shears: The Role of Cold Pools. *Journal of the Atmospheric Sciences*, 58(13):1650–1672, 2001.

Wolfgang Langhans and David M Romps. The origin of water vapor rings in tropical oceanic cold pools. *Geophysical Research Letters*, 42(18):7825–7834, 2015. doi:https://doi.org/10.1002/2015GL065623.

Simon P de Szoeke, Eric D Skyllingstad, Paquita Zuidema, and Arunchandra S Chandra. Cold pools and their influence on the tropical marine boundary layer. *Journal of the Atmospheric Sciences*, 74(4):1149–1168, 2017. doi:https://doi.org/10.1175/JAS-D-16-0264.1.

Franziska Glassmeier and Graham Feingold. Network approach to patterns in stratocumulus clouds. *Proceedings of the National Academy of Sciences*, 114(40):10578–10583, 2017. doi:https://doi.org/10.1073/pnas.1706495114.

Carlo Cafaro and Gabriel G Rooney. Characteristics of colliding density currents: A numerical and theoretical study. *Quarterly Journal of the Royal Meteorological Society*, 144(715):1761–1771, 2018. doi:https://doi.org/10.1002/qj.3337.

This article is protected by copyright. All rights reserved.

Accepted Article

Herman F. Fuglestvedt and Jan O. Haerter. Cold Pools as Conveyor Belts of Moisture. *Geophysical Research Letters*, 47(12): 1–11, 2020. doi:https://doi.org/10.1029/2020GL087319.

Jean-Yves Grandpeix and Jean-Philippe Lafore. A density current parameterization coupled with Emanuel's convection scheme. Part I: The models. *Journal of the Atmospheric Sciences*, 67(4):881–897, 2010. doi:https://doi.org/10.1175/2009JAS3044.1.

Steven J Böing. An object-based model for convective cold pool dynamics. *Mathematics of Climate and Weather Forecasting*, 2(1), 2016. doi:https://doi.org/10.1515/mcwf-2016-0003.

Julia Miriam Windmiller. *Organization of tropical convection.* PhD thesis, Ludwig-Maximilian University, Munich, Germany, 2017.

Jan O Haerter, Bettina Meyer, and Silas Boye Nissen. Diurnal self-aggregation. *npj Climate and Atmospheric Science*, 3(30): 1–11, 2020. doi:https://doi.org/10.1038/s41612-020-00132-z.

Jan O Haerter, Steven J Böing, Olga Henneberg, and Silas Boye Nissen. Circling in on convective organization. *Geophysical Research Letters*, 46(12):7024–7034, 2019. doi:https://doi.org/10.1029/2019GL082092.

Joseph Smagorinsky. General circulation experiments with the primitive equations: I. the basic experiment. *Monthly weather review*, 91(3):99–164, 1963.

Robert Pincus and Bjorn Stevens. Monte Carlo spectral integration: A consistent approximation for radiative transfer in large eddy simulations. *Journal of Advances in Modeling Earth Systems*, 1(2):1–9, 2009. doi: https://doi.org/10.3894/JAMES.2009.1.1.

Bjorn Stevens, Chin-Hoh Moeng, Andrew S Ackerman, Christopher S Bretherton, Andreas Chlond, Stephan de Roode, James Edwards, Jean-Christophe Golaz, Hongli Jiang, Marat Khairoutdinov, Michael P. Kirkpatrick, David C. Lewellen, Adrian Lock, Frank Mller, David E. Stevens, Eoin Whelan, and Ping Zhu. Evaluation of large-eddy simulations via observations of nocturnal marine stratocumulus. *Monthly Weather Review*, 133(6):1443–1462, 2005. doi:https://doi.org/10.1175/MWR2930.1.

A Seifert and KD Beheng. A two-moment cloud microphysics parameterization for mixed-phase clouds. Part 1: Model description. *Meteorology and Atmospheric Physics*, 92(1-2):45–66, 2006. doi:https://doi.org/10.1007/s00703-005-0113-3.

Olga Henneberg, Bettina Meyer, and Jan O Haerter. Particle-based tracking of cold pool gust fronts. *Journal of Advances in Modeling Earth Systems*, 12(5):e2019MS001910, 2020. doi:https://doi.org/10.1029/2019MS001910.

George C Craig and Julia M Mack. A coarsening model for self-organization of tropical convection. *Journal of Geophysical Research: Atmospheres*, 118(16):8761–8769, 2013. doi:https://doi.org/10.1002/jgrd.50674.

Julia M Windmiller and George C Craig. Universality in the Spatial Evolution of Self-Aggregation of Tropical Convection. *Journal of Atmospheric Sciences*, 76(6):1677–1696, 2019. doi:https://doi.org/10.1175/JAS-D-18-0129.1.

Christopher Moseley, Olga Henneberg, and Jan O Haerter. A statistical model for isolated convective precipitation events. *Journal of Advances in Modeling Earth Systems*, 11(1):360–375, 2019. doi:https://doi.org/10.1029/2018MS001383.

Peter G Black. Mesoscale cloud patterns revealed by apollo-soyuz photographs. *Bulletin of the American Meteorological Society*, 59(11):1409–1419, 1978.

Paquita Zuidema, Zhujun Li, Reginald J Hill, Ludovic Bariteau, Bob Rilling, Chris Fairall, W Alan Brewer, Bruce Albrecht, and Jeff Hare. On trade wind cumulus cold pools. *Journal of the Atmospheric Sciences*, 69(1):258–280, 2012. doi: https://doi.org/10.1175/JAS-D-11-0143.1.

Zhe Feng, Samson Hagos, Angela K Rowe, Casey D Burleyson, Matus N Martini, and Simon P Szoeke. Mechanisms of convective cloud organization by cold pools over tropical warm ocean during the amie/dynamo field campaign. *Journal of Advances in Modeling Earth Systems*, 7(2):357–381, 2015. doi:https://doi.org/10.1002/2014MS000384.

Christopher Moseley, Peter Berg, and Jan O Haerter. Probing the precipitation life cycle by iterative rain cell tracking. *Journal of Geophysical Research: Atmospheres*, 118(24):13–361, 2013. doi:https://doi.org/10.1002/2013JD020868.

Aryeh J Drager and Susan C van den Heever. Characterizing convective cold pools. *Journal of Advances in Modeling Earth Systems*, 9(2):1091–1115, 2017. doi:https://doi.org/10.1002/2016MS000788.

This article is protected by copyright. All rights reserved.

Accepted Article

425 Marielle B Fournier and Jan O Haerter. Tracking the gust fronts of convective cold pools. *Journal of Geophysical Research:*
426 *Atmospheres*, 124(21):11103–11117, 2019. doi:https://doi.org/10.1029/2019JD030980.
427 Adrian M Tompkins and Addisu G Semie. Organization of tropical convection in low vertical wind shears: Role of updraft en-
428 trainment. *Journal of Advances in Modeling Earth Systems*, 9(2):1046–1068, 2017. doi:https://doi.org/10.1002/2016MS000802.
429 Mirjam Hirt, George C Craig, Sophia AK Schäfer, Julien Savre, and Rieke Heinze. Cold pool driven convective initiation:
430 using causal graph analysis to determine what convection permitting models are missing. *Quarterly Journal of the Royal*
431 *Meteorological Society*, 146(730):2205–2227, 2020. doi:https://doi.org/10.1002/qj.3788.
432 Caroline J Muller and Isaac M Held. Detailed investigation of the self-aggregation of convection in cloud-resolving simulations.
433 *Journal of the Atmospheric Sciences*, 69(8):2551–2565, 2012. doi:https://doi.org/10.1175/JAS-D-11-0257.1.
434 Kerry Emanuel, Allison A Wing, and Emmanuel M Vincent. Radiative-convective instability. *Journal of Advances in Modeling*
435 *Earth Systems*, 6(1):75–90, 2014.
436 James FW Purdom. Some uses of high-resolution goes imagery in the mesoscale forecasting of convection and its behavior.
437 *Monthly Weather Review*, 104(12):1474–1483, 1976.
438 John F Weaver and Stephan P Nelson. Multiscale aspects of thunderstorm gust fronts and their effects on subsequent storm
439 development. *Monthly Weather Review*, 110(7):707–718, 1982.
440 Giuseppe Torri and Zhiming Kuang. On Cold Pool Collisions in Tropical Boundary Layers. *Geophysical Research Letters*, 46
441 (1):399–407, 2019. doi:https://doi.org/10.1029/2018GL080501.
442 Jan O Haerter. Convective Self-Aggregation As a Cold Pool-Driven Critical Phenomenon. *Geophysical Research Letters*, 46(7):
443 4017–4028, 2019. doi:https://doi.org/10.1029/2018GL081817.
444 Leah D Grant and Susan C van den Heever. Cold pool dissipation. *Journal of Geophysical Research: Atmospheres*, 121(3):
445 1138–1155, 2016. doi:https://doi.org/10.1002/2015JD023813.
446 Leah D Grant and Susan C van den Heever. Cold Pool-Land Surface Interactions in a Dry Continental Environment. *Journal*
447 *of Advances in Modeling Earth Systems*, 10(7):1513–1526, 2018. doi:https://doi.org/10.1029/2018MS001323.
448 Julia M Windmiller and Cathy Hohenegger. Convection on the Edge. *Journal of Advances in Modeling Earth Systems*, 11(12):
449 3959–3972, 2019.
450 David Coppin and Sandrine Bony. Physical mechanisms controlling the initiation of convective self-aggregation
451 in a general circulation model. *Journal of Advances in Modeling Earth Systems*, 7(4):2060–2078, 2015. doi:
452 https://doi.org/10.1002/2015MS000571.
453 Isaac M Held and Brian J Soden. Robust responses of the hydrological cycle to global warming. *Journal of Climate*, 19(21):
454 5686–5699, 2006. doi:https://doi.org/10.1175/JCLI3990.1.

Accepted Article

This article is protected by copyright. All rights reserved.